PERGAMON

International Journal of Heat and Mass Transfer 42 (1999) 3217–3230

International Journal of HEAT and MASS TRANSFER

A low Reynolds number two-equation k_θ–$\tilde{\epsilon}_\theta$ model to predict thermal fields

C.B. Hwang, C.A. Lin*

Department of Power Mechanical Engineering, National Tsing Hua University, Hsinchu, Taiwan 30043

Received 26 March 1998; received in revised form 7 December 1998

Abstract

An improved low Reynolds number k_θ–$\tilde{\epsilon}_\theta$ turbulence model is proposed to model the thermal field without the explicit prescription of the turbulent Prandtl number. The model is designed to conform with the near-wall characteristics obtained with direct numerical simulation data, but also to possess correct asymptotic behavior in the vicinity of the wall. The asymptotic limits of equations, governing the temperature variance (k_θ) and its dissipation rate ($\tilde{\epsilon}_\theta$), are satisfied by the incorporation of the viscous dissipation related terms. The performance of the proposed model is evaluated by applying to fully developed channel flows with and without wall transpiration, and the thermal entrance region of a duct. The computations are validated against measurements and direct numerical simulation data and the predicted results indicate that the proposed model is capable of reproducing the complex near-wall thermal field considered.

1. Introduction

In predicting the turbulent heat transfer, the most commonly adopted approach is to model the turbulent heat flux with the Boussinesq approximation and the thermal diffusivity is usually adopted to be proportional to the ratio of the turbulent viscosity and a constant turbulent Prandtl number. This approach assumes that a direct analogy between eddy diffusivities of momentum and heat exists. However, the detailed dynamic and thermal field data from the direct numerical simulation indicated that the turbulent Prandtl number varied over a broad range across the flowfield [1,2], contrary to the commonly assumed constant value. It was further argued that in order to calculate the turbulent heat transfer in wall shear flows correctly, the constant turbulent Prandtl number assumption has to be relaxed [3]. Therefore, it is highly desirable to formulate a turbulent heat transfer model which is capable of adapting the variation of turbulent Prandtl number in response to the variation of Prandtl number and flow structure in a wide range of complex flows.

One approach is to solve the transport equations of heat flux directly. However, this requires the adoption of Reynolds stress model in the dynamic field and the modelling of the heat flux equation is complex and not always straightforward. An alternative is to adopt the gradient transport of heat fluxes and the thermal diffusivity is made function of dynamic and thermal time scales. This is achieved through the solution of two additional equations which govern the transport of temperature variance and its dissipation rate. This approach avoids the prescription of the turbulent Prandtl number, explicitly.

It was indicated [4] that a marked improvement over the wall function approach in predicting the local heat

* Corresponding author.

0017-9310/99/$ - see front matter
PII: S0017-9310(98)00382-2

Nomenclature

b, c, d	constant
C	model constant
$\mathscr{C}$	convection term
C_f	friction coefficient, $\tau_w/(\rho U_m^2/2)$
C_p	specific heat at constant pressure
$\mathscr{D}$	viscous diffusion term
F	injection rate, v_0/U_m
f	damping function
f_λ	wall-damping function for turbulent heat diffusivity
f_μ	wall-damping function for eddy-viscosity equation
h	channel height
k	turbulent kinetic energy
k_θ	temperature variance
Nu	Nusselt number
P	mean pressure
$\mathscr{P}$	production term
Pr	Prandtl number
q_w	wall heat flux
R	time scale ratio, $(k_\theta/\tilde{\epsilon}_\theta)/(k/\epsilon)$
R_t	turbulent Reynolds numbers, $k^2/\nu\tilde{\epsilon}$
Re_τ	Reynolds numbers based on the wall friction velocity, $U_\tau\delta/\nu$
S_θ	viscous dissipation term, $\mu(\frac{\partial U_i}{\partial x_j}+\frac{\partial U_j}{\partial x_i})\frac{\partial U_i}{\partial x_j}$
$\mathscr{T}$	turbulent diffusion term
U	mean velocity
U_τ	friction velocity, $\sqrt{\tau_w/\rho}$
u	fluctuation velocity
v_0	wall-normal velocity
x	physical coordinate of the orthogonal grid
y	distance normal to the wall
y^+	dimensionless wall coordinate, yU_τ/ν.

Greek symbols

α	thermal diffusivity
γ	dissipation term
δ	half channel height, $\frac{1}{2}h$
δ_{ij}	Kronecker delta
ϵ	total turbulent dissipation rate
$\tilde{\epsilon}$	isotropic dissipation rate
$\hat{\epsilon}$	'wall' dissipation, $\epsilon-\tilde{\epsilon}$
ϵ_θ	dissipation rate of temperature variance
Θ	mean temperature
Θ_τ	friction temperature, $q_w/\rho C_p U_\tau$
θ	fluctuating temperature
μ	dynamic viscosity
ν	kinematic viscosity, μ/ρ
Π	pressure diffusion term
ρ	mean density
σ	Prandtl number
τ_m	mixing time scale
τ_w	wall shear stress.

Subscripts

b, t	bottom/top wall
i, j, k	tensorial direction indices
i, s	injection/suction side
m	bulk mean
0	inlet condition
t	turbulent
w	at the wall
θ	for thermal field
λ	normalized on Taylor microscale.

Superscripts

$+$	non-dimensionless quantities
$'$	fluctuations.

Mathematical symbol

$\overline{(\ )}$	time-averaged value.

transfer coefficients can be achieved by the applications of the low Reynolds number turbulence models in the near-wall region. This is partly due to the sufficiently resolved turbulence transport processes and consequently the heat transfer characteristics in the vicinity of the wall. Especially in high Prandtl number fluids, the conductive sublayer is so thin that the turbulent heat transfer is more affected by the velocity fluctuations in the viscous sublayer.

Several proposals [3,5] had been made, but due to the lack of detailed and reliable measurements of the near-wall dynamic and thermal structure, the forms of the model were based on ad hoc adjustments of the model constants and damping functions to reproduce the dynamic and thermal fields. One commonly found defect of the models is the adoption of y^+ in the damping function which is known to cause problem in the separating flows where at the reattachment point the wall shear stress is zero.

The arrival of direct numerical simulation (DNS) [1,6–8] shed some light on the detailed flow structure in the near-wall region, and the detailed energy budgets derived from the DNS data provide a route towards the modelling of wall turbulence. Further, the asymptotic analysis, which is supported by DNS data, provides a powerful tool in analyzing the forms of the models. However, few of the many proposed models completely satisfy the asymptotic limit and the DNS data. For example, it was commonly found that the predicted dissipation rate of temperature variance (ϵ_θ) reached its maximum value somewhere inside the viscous sub-layer [3]. However DNS data indicate that the local maximum value of dissipation rate of temperature variance should be located at the wall itself.

The aforementioned defect of the model predictions is also frequently encountered in the prediction of a turbulence kinetic energy dissipation rate in which most turbulence models predicted a mislocated local maximum at the wall [9]. Based on the DNS data and asymptotic analysis, Kawamura [10] argued that the traditionally modelled equations for turbulent kinetic energy and its dissipation rate are not balanced in the asymptotic state and that the inclusion of pressure diffusion was found essential. This has motivated Hwang and Lin [9] to propose a low Reynolds number k–$\tilde{\epsilon}$ model for the dynamic fields. Key features of the model are the adoption of the Taylor microscale in the damping function and the inclusion of pressure diffusion terms in the turbulent kinetic energy (k) and dissipation rate ($\tilde{\epsilon}$) equations.

In the present paper, the similar approach is employed to analyze the k_θ and $\tilde{\epsilon}_\theta$ equations and an improved and unsophisticated model is proposed to model the thermal field. Cases considered are fully developed channel flows, with and without wall transpiration, and the thermal entrance region of a duct. For the transpired flows, even though the magnitude of the transpiration rate is low compared to the mainstream, it significantly changes the surface skin friction as well as turbulence quantities near the wall. This complex dynamic and thermal field possess severe test of the model, and the developing thermal field within the fully developed flow provides a critical evaluation of the model performance due to that the dynamic and thermal fields are not similar, and hence the Reynolds analogy is strictly not applicable. These computations are validated against measurements and direct numerical simulation data.

2. Governing equations

The Reynolds-averaged continuity, Navier–Stokes and temperature equations can be written as,

$$\frac{\partial U_j}{\partial x_j} = 0 \tag{1}$$

$$\frac{\partial U_j U_i}{\partial x_j} = -\frac{1}{\rho}\frac{\partial P}{\partial x_i} + \frac{\partial}{\partial x_j}\left[\nu\left(\frac{\partial U_i}{\partial x_j} + \frac{\partial U_j}{\partial x_i}\right) - \overline{u_i u_j}\right] \tag{2}$$

$$\frac{\partial U_j \Theta}{\partial x_j} = \frac{\partial}{\partial x_j}\left[\frac{\nu}{\sigma}\frac{\partial \Theta}{\partial x_j} - \overline{u_j\theta}\right] + \frac{1}{\rho C_p}(S_\theta + \overline{S'_\theta}) \tag{3}$$

where ν and σ are kinematic viscosity and Prandtl numbers, respectively.

$$S_\theta = \mu\left(\frac{\partial U_i}{\partial x_j} + \frac{\partial U_j}{\partial x_i}\right)\frac{\partial U_i}{\partial x_j}$$

and

$$\overline{S'_\theta} = \overline{\mu\left(\frac{\partial u_i}{\partial x_j} + \frac{\partial u_j}{\partial x_i}\right)\frac{\partial u_i}{\partial x_j}} \equiv \rho\epsilon$$

denote the viscous dissipation terms [11].

In the temperature equation, the viscous dissipation term is generally small in the high Reynolds number regime of the flow field and is often neglected. However, the near wall viscous dissipation might be high, especially in the high speed flow, and this term should be retained for more analysis.

Within the framework of eddy-viscosity and adopting Boussinesq approximation, the Reynolds stress and heat flux are approximated as,

$$-\overline{u_i u_j} = \nu_t\left(\frac{\partial U_i}{\partial x_j} + \frac{\partial U_j}{\partial x_i}\right) - \frac{2}{3}\delta_{ij}k \tag{4}$$

$$-\overline{u_j\theta} = \alpha_t\frac{\partial \Theta}{\partial x_j} \tag{5}$$

where ν_t and α_t are turbulent kinematic viscosity and thermal diffusivity, respectively.

In the present applications, the turbulence model adopted is the $k-\epsilon$ [12] and $k_\theta-\epsilon_\theta$ model [5]. When applying the model towards the wall, the contribution of molecular viscosity on the shear stress increases, and the standard high Reynolds number turbulence model must be modified to account for the diminishing effect of the near-wall turbulence levels. The construction of the low Reynolds number model is the focus of the next section.

3. Near-wall modelling

3.1. $k-\tilde{\epsilon}$ model for dynamic field

In the present approach the turbulence is described by the eddy viscosity model which solves the transport equations for turbulent kinetic energy and turbulent dissipation rate. The present approach decomposes the dissipation rate into two parts, i.e. $\epsilon = \tilde{\epsilon} + \hat{\epsilon}$, and adopting $\tilde{\epsilon}$ as the dependent variable, and $\hat{\epsilon}$ is defined as: $\hat{\epsilon} = 2\nu(\partial\sqrt{k}/\partial x_j)^2$. The advantage of this approach is that $\tilde{\epsilon}$ reaches zero at the wall, i.e. $\epsilon_w = \hat{\epsilon}_w = 2\nu(\partial\sqrt{k}/\partial x_j)^2_w$ [12], and $\tilde{\epsilon}$ equals ϵ at about $y^+ > 15$.

The adopted model is designed to conform with the near-wall characteristics obtained with direct numerical simulation data, but also to possess correct asymptotic behavior in the vicinity of the wall. Key features of the model are the adoption of Taylor microscale in the damping function and the inclusions of the pressure diffusion terms [10] in both k and $\tilde{\epsilon}$ equations which ensure the asymptotic limits to be satisfied. Based on the above approach, an improved low Reynolds number $k-\tilde{\epsilon}$ model [9] was proposed and takes the form as,

$$\nu_t = 0.09 f_\mu \frac{k^2}{\tilde{\epsilon}} \tag{6}$$

$$\begin{aligned}\frac{\partial U_j k}{\partial x_j} &= \frac{\partial}{\partial x_j}\left[\nu\frac{\partial k}{\partial x_j}\right] + \frac{\partial}{\partial x_j}\left[\frac{\nu_t}{\sigma_k}\frac{\partial k}{\partial x_j}\right] \\ &\quad - \frac{1}{2}\nu\frac{\partial}{\partial x_j}\left[\frac{k}{\epsilon}\frac{\partial \hat{\epsilon}}{\partial x_j}\right] - \overline{u_i u_j}\frac{\partial U_i}{\partial x_j} - (\tilde{\epsilon} + \hat{\epsilon})\end{aligned} \tag{7}$$

$$\begin{aligned}\frac{\partial U_j \tilde{\epsilon}}{\partial x_j} &= \frac{\partial}{\partial x_j}\left[\nu\frac{\partial \tilde{\epsilon}}{\partial x_j}\right] + \frac{\partial}{\partial x_j}\left[\frac{\nu_t}{\sigma_\epsilon}\frac{\partial \tilde{\epsilon}}{\partial x_j}\right] \\ &\quad - \nu\frac{\partial}{\partial x_j}\left[\frac{\tilde{\epsilon}}{k}\frac{\partial k}{\partial x_j}\right] - 1.44\overline{u_i u_j}\frac{\partial U_i}{\partial x_j}\frac{\tilde{\epsilon}}{k} - 1.92\frac{\tilde{\epsilon}^2}{k}\end{aligned} \tag{8}$$

where $y_\lambda = y/\sqrt{\nu k/\tilde{\epsilon}}$ and $\sqrt{\nu k/\tilde{\epsilon}}$ is the Taylor microscale. The damping functions of the model are set to be:

$$f_\mu = 1 - \exp(-0.01 y_\lambda - 0.008 y_\lambda^3)$$

$$\sigma_k = 1.4 - 1.1\exp\left(-\frac{y_\lambda}{10}\right)$$

$$\sigma_\epsilon = 1.3 - 1.0\exp\left(-\frac{y_\lambda}{10}\right).$$

The adoption of y_λ avoids the obvious defect, i.e. the singularity occurring at the reattaching point by adopting $y^+ = U_\tau y/\nu$. Practically, $y_\lambda = y/\sqrt{\nu k/\tilde{\epsilon}} =$

$y/[(k^{3/2}/\tilde{\epsilon})/R_t^{1/2}]$ could serve as a length-scale damping factor when approaching the wall, and accounts for the wall-proximity size of eddies which are of the order of the wall distance, y. Simultaneously the damping functions above are chosen to retain the high Reynolds number form away from solid boundaries. The asymptotic values of turbulent Prandtl number σ_k and σ_ϵ are adopted as 0.3 [9,13] to obtain sufficient dissipation rate in the vicinity of the wall. In the core region of the flow, $\sigma_k > \sigma_\epsilon$ is chosen to eliminate the common drawback that turbulent diffusion of k overwhelms that of ϵ [14].

3.2. k_θ–$\tilde{\epsilon}_\theta$ model for thermal field

By adopting the Boussinesq approximation, the turbulent heat flux can be approximated as,

$$-\overline{u_j\theta} = \alpha_t \frac{\partial \Theta}{\partial x_j}$$

and the thermal diffusivity is traditionally modelled as,

$$\alpha_t = \frac{\nu_t}{Pr_t}$$

where Pr_t is the turbulent Prandtl number. This approach requires the explicit prescription of the value of the turbulent Prandtl number and the commonly adopted approach is to assume a constant value which was generally taken to be 0.9 [12]. However, as indicated in the direct numerical simulation data [1,2], the turbulent Prandtl number is not constant, and the thermal diffusivity is not necessarily related to the eddy diffusivity [5].

Alternatively, based on the dimensional approach, the thermal diffusivity, α_t, can be expressed as a function of velocity scale ($k^{1/2}$) and the mixing time-scale (τ_m) [5,15],

$$\alpha_t \equiv \frac{\nu_t}{Pr_t} = C_\lambda f_\lambda k^{1/2} k^{1/2} \tau_m \tag{9}$$

where the form of τ_m varies, but usually is deemed to be a function of

$$R = \frac{k_\theta}{\tilde{\epsilon}_\theta} \Big/ \cdot \frac{k}{\tilde{\epsilon}},$$

which is the ratio of the thermal and mechanical time-scales. $k_\theta = \overline{\theta^2}/2$ is the half variance of temperature and $\tilde{\epsilon}_\theta = \alpha(\partial\theta/\partial x_j)^2 - 2\alpha(\partial\sqrt{k_\theta}/\partial x_j)^2$ is the dissipation rate of the variance of temperature.

In the present approach, the form of the mixing time scale adopted is $\tau_m = k/\tilde{\epsilon}\sqrt{Pr/R}$, which is designed to well reproduce the DNS data in the core region [16]. At the same time it requires the solution of two extra transport equations k_θ and $\tilde{\epsilon}_\theta$ and the construction of the modelled equations are detailed below.

The equation for half temperature variance $k_\theta = \overline{\theta^2}/2$ equation takes the form [11],

$$\underbrace{\frac{\partial U_j k_\theta}{\partial x_j}}_{\mathscr{C}_{k_\theta}} = \underbrace{\frac{\partial}{\partial x_j}\left[\alpha \frac{\partial k_\theta}{\partial x_j}\right]}_{\mathscr{D}_{k_\theta}} + \underbrace{\frac{\partial}{\partial x_j}\left[\frac{\alpha_t}{\sigma_{k_\theta}} \frac{\partial k_\theta}{\partial x_j}\right]}_{\mathscr{T}_{k_\theta}} + \underbrace{\frac{1}{\rho C_p}\overline{\theta S'_\theta}}_{\Pi_{k_\theta}} - \underbrace{\overline{u_j\theta}\frac{\partial \Theta}{\partial x_j}}_{\mathscr{P}_{k_\theta}} - \underbrace{(\tilde{\epsilon}_\theta + \hat{\epsilon}_\theta)}_{\epsilon_\theta} \tag{10}$$

Before examining the asymptotic behavior of the individual terms in the above equation, it is beneficial to look into the asymptotic values of the instantaneous components with respect to wall distance y,

$$\theta = b_4 y + c_4 y^2 + d_4 y^3 + \cdots$$

$$k_\theta \equiv \frac{\overline{\theta^2}}{2} = \frac{1}{2}\overline{b_4^2} y^2 + \overline{b_4 c_4} y^3 + \cdots$$

$$= \frac{1}{2} b_\theta y^2 + c_\theta y^3 + d_\theta y^4 + \cdots$$

$$\epsilon_\theta \equiv \alpha \overline{\left(\frac{\partial \theta}{\partial x_j}\right)^2} = \alpha b_\theta + 4\alpha c_\theta y + d_\phi y^2 + \cdots$$

$$\hat{\epsilon}_\theta = 2\alpha\left(\frac{\partial \sqrt{k_\theta}}{\partial x_j}\right)^2 = \alpha b_\theta + 4\alpha c_\theta y + \hat{d}_\phi y^2 + \cdots$$

$$\tilde{\epsilon}_\theta = \epsilon_\theta - \hat{\epsilon}_\theta = (d_\phi - \hat{d}_\phi) y^2 + \cdots$$

The above variations are based on the isothermal wall condition and hence vanishing temperature fluctuation is assumed to prevail at the wall [15]. By inserting the y dependent quantities into the k_θ equation, it can be easily verified that the dominant terms in the vicinity of the wall are,

$$\mathscr{D}_{k_\theta} = \alpha b_\theta + 6\alpha c_\theta y + 12\alpha d_\theta y^2 + \cdots \tag{11}$$

$$-\epsilon_\theta = -\alpha b_\theta - 4\alpha c_\theta y - d_\phi y^2 + \cdots \tag{12}$$

$$\Pi_{k_\theta} \propto y. \tag{13}$$

To keep the asymptotic limits balanced up to the first order term, the viscous dissipation function term, Π_{k_θ}, can be modelled as,

$$\Pi_{k_\theta} = -\frac{1}{2}\alpha\frac{\partial}{\partial x_j}\left[\frac{k_\theta}{\epsilon_\theta}\frac{\partial\hat{\epsilon}_\theta}{\partial x_j}\right] = -2\alpha c_\theta y + \cdots \tag{14}$$

This ensures the satisfaction of the asymptotic limit in the transport equation up to the first order term in the near wall region.

Next, attention is directed to the equation governing the dissipation rate of temperature variance. The exact equation for temperature variance dissipation rate $\epsilon_\theta = \alpha(\partial\theta/\partial x_j)^2$ equation takes the form [11],

$$\begin{aligned}\frac{\partial U_j\epsilon_\theta}{\partial x_j} &= \frac{\partial}{\partial x_j}\left[\alpha\frac{\partial\epsilon_\theta}{\partial x_j}\right] - \frac{\partial}{\partial x_j}(\overline{u_j\epsilon'_\theta}) - 2\alpha\left[\overline{\frac{\partial\theta}{\partial x_i}\frac{\partial u_j}{\partial x_i}\frac{\partial\theta}{\partial x_j}} + \overline{\frac{\partial u_j}{\partial x_i}\frac{\partial\theta}{\partial x_i}}\frac{\partial\Theta}{\partial x_j} + \overline{\frac{\partial\theta}{\partial x_i}\frac{\partial\theta}{\partial x_j}}\frac{\partial U_i}{\partial x_j}\right]\\ &\quad - 2\overline{\left(\frac{\partial^2\theta}{\partial x_i\partial x_j}\right)^2} - 2\alpha\overline{u_i\frac{\partial\theta}{\partial x_j}}\frac{\partial^2\Theta}{\partial x_i\partial x_j} + \frac{2\alpha}{\rho C_p}\overline{\frac{\partial S'_\theta}{\partial x_j}\frac{\partial\theta}{\partial x_j}}\end{aligned} \tag{15}$$

Here, similar to that adopted in the k–$\tilde{\epsilon}$ modelling, the ϵ_θ is decomposed into two terms, i.e. $\epsilon_\theta = \hat{\epsilon}_\theta + \tilde{\epsilon}_\theta$ and $\tilde{\epsilon}_\theta$ is adopted as the dependent variable. Again, the advantage of this choice is that the value of $\tilde{\epsilon}_\theta$ is zero right at the wall, because at the wall ϵ_θ is equal to $\hat{\epsilon}_\theta$. The transport equation of $\tilde{\epsilon}_\theta$ is generally modelled as [5],

$$\underbrace{\frac{\partial U_j\tilde{\epsilon}_\theta}{\partial x_j}}_{\mathscr{C}_{\epsilon_\theta}} = \underbrace{\frac{\partial}{\partial x_j}\left[\alpha\frac{\partial\tilde{\epsilon}_\theta}{\partial x_j}\right]}_{\mathscr{D}_{\epsilon_\theta}} + \underbrace{\frac{\partial}{\partial x_j}\left[\frac{\alpha_t}{\sigma_{\epsilon_\theta}}\frac{\partial\tilde{\epsilon}_\theta}{\partial x_j}\right]}_{\mathscr{T}_{\epsilon_\theta}} \underbrace{-C_{P_1}f_{P_1}\frac{\tilde{\epsilon}_\theta}{2k_\theta}\overline{u_j\theta}\frac{\partial\Theta}{\partial x_j} - C_{P_2}f_{P_2}\frac{\tilde{\epsilon}_\theta}{k}\overline{u_iu_j}\frac{\partial U_i}{\partial x_j}}_{\mathscr{P}_{\epsilon_\theta}} \underbrace{-C_{D_1}f_{D_1}\frac{\tilde{\epsilon}_\theta^2}{2k_\theta} - C_{D_2}f_{D_2}\frac{\tilde{\epsilon}\tilde{\epsilon}_\theta}{k} + \Pi_{\epsilon_\theta}}_{\gamma_{\epsilon_\theta}} \tag{16}$$

In the vicinity of the wall, convection $\mathscr{C}_{\epsilon_\theta}$, turbulent diffusion $\mathscr{T}_{\epsilon_\theta}$, production $\mathscr{P}_{\epsilon_\theta}$ and dissipation γ_{ϵ_θ} terms go to zero very rapidly. The asymptotic behaviors of the remaining terms are:

$$\mathscr{D}_{\epsilon_\theta} \equiv \frac{\partial}{\partial x_j}\left[\alpha\frac{\partial\tilde{\epsilon}_\theta}{\partial x_j}\right] = 2\alpha[d_\phi - \hat{d}_\phi] + \cdots \tag{17}$$

$$\Pi_{\epsilon_\theta} \propto \mathscr{O}(1) \tag{18}$$

and the function Π_{ϵ_θ} could be modelled as

$$\Pi_{\epsilon_\theta} \equiv -\alpha\frac{\partial}{\partial x_j}\left[\frac{\tilde{\epsilon}_\theta}{k_\theta}\frac{\partial k_\theta}{\partial x_j}\right] = -2\alpha[d_\phi - \hat{d}_\phi] + \cdots \tag{19}$$

Here the inclusion of the Π_{ϵ_θ} term just compensates $\mathscr{D}_{\epsilon_\theta}$ and renders the satisfaction of the asymptotic limits in the vicinity of the wall.

3.2.1. The proposed k_θ–$\tilde{\epsilon}_\theta$ model

The proposed forms of the temperature variance (k_θ) and its dissipation rate ($\tilde{\epsilon}_\theta$) equations are,

$$\alpha_t = C_\lambda f_\lambda\frac{k^2}{\tilde{\epsilon}}\sqrt{\frac{Pr}{\frac{k_\theta}{\tilde{\epsilon}_\theta}/\frac{k}{\tilde{\epsilon}}}} \tag{20}$$

$$\begin{aligned}\frac{\partial U_jk_\theta}{\partial x_j} &= \frac{\partial}{\partial x_j}\left[\alpha\frac{\partial k_\theta}{\partial x_j}\right] + \frac{\partial}{\partial x_j}\left[\frac{\alpha_t}{\sigma_{k_\theta}}\frac{\partial k_\theta}{\partial x_j}\right]\\ &\quad - \frac{1}{2}\alpha\frac{\partial}{\partial x_j}\left[\frac{k_\theta}{\epsilon_\theta}\frac{\partial\hat{\epsilon}_\theta}{\partial x_j}\right] - \overline{u_j\theta}\frac{\partial\Theta}{\partial x_j} - (\tilde{\epsilon}_\theta + \hat{\epsilon}_\theta)\end{aligned} \tag{21}$$

$$\begin{aligned}\frac{\partial U_j\tilde{\epsilon}_\theta}{\partial x_j} &= \frac{\partial}{\partial x_j}\left[\alpha\frac{\partial\tilde{\epsilon}_\theta}{\partial x_j}\right] + \frac{\partial}{\partial x_j}\left[\frac{\alpha_t}{\sigma_{\epsilon_\theta}}\frac{\partial\tilde{\epsilon}_\theta}{\partial x_j}\right]\\ &\quad -\alpha\frac{\partial}{\partial x_j}\left[\frac{\tilde{\epsilon}_\theta}{k_\theta}\frac{\partial k_\theta}{\partial x_j}\right] - C_{P_1}f_{P_1}\frac{\tilde{\epsilon}_\theta}{2k_\theta}\overline{u_j\theta}\frac{\partial\Theta}{\partial x_j}\\ &\quad - C_{P_2}f_{P_2}\frac{\tilde{\epsilon}_\theta}{k}\overline{u_iu_j}\frac{\partial U_i}{\partial x_j} - C_{D_1}f_{D_1}\frac{\tilde{\epsilon}_\theta^2}{2k_\theta}\\ &\quad - C_{D_2}f_{D_2}\frac{\tilde{\epsilon}\tilde{\epsilon}_\theta}{k}.\end{aligned} \tag{22}$$

The coefficients and the damping functions adopted are,

$$C_\lambda = 0.1$$

$$f_\lambda = 1 - \exp(-0.008y_\lambda - 0.004y_\lambda^2 - 0.005Pr^{1/4}y_\lambda^3)$$

$$C_{P1} = 1.8 \quad f_{P1} = 1 - \exp\left(-\frac{y_\lambda}{2}\right)$$

$$C_{P2} = 0.68 + 3.5\exp(-4.7Pr) \quad f_{P2} = 1$$

$$C_{D1} = 2.2 \quad f_{D1} = 1 - \frac{1}{4.4}\exp\left(-\frac{R_t}{60}\right)$$

$$C_{D2} = 0.8 \quad f_{D2} = 1$$

$$\sigma_{k_\theta} = \sigma_k$$

$$\sigma_{\epsilon_\theta} = \sigma_\epsilon.$$

The constants in the model are chosen so that the present model retains its high Reynolds number form [5,17] away from solid boundaries. According to the work of Elghobashi and Launder [17], it was indicated that the set of coefficients,

C_{P1}	C_{D1}	C_{D2}
1.8	2.2	0.8

not only gave a satisfactory account of the decay of temperature fluctuation, but also delivered better results for the thermal mixing layers. These are the coefficients adopted in the present study. The same coefficients were also adopted in the work of Nagano and Kim [5] and Sommer et al. [3]. The coefficient f_{D1} is approximated as a function of turbulence Reynolds number, defined as $R_t = k^2/\nu\tilde{\epsilon}$ as suggested in [18]. The near wall asymptotic values, 0.3, of the turbulent diffusion coefficients σ_{k_θ} and σ_{ϵ_θ}, are determined according to the analysis of the DNS data [19] in the vicinity of the wall.

The adopted form of viscous damping function f_λ reproduces correctly the asymptotic limit, i.e. $f_\lambda \propto y$ and hence $-\overline{v\theta} \propto y^3$ towards the wall. The asymptotic satisfaction accomplishes the correct levels of ϵ_θ with the maximum locating at the wall itself. This modification is important to properly mimic the turbulence levels and transfer rates toward the surface wall.

4. Numerical procedure

This scheme solves discretised versions of all equations over a staggered finite-volume arrangement [20]. The principle of mass–flux continuity is imposed indirectly via the solution of pressure–correction equations according to the SIMPLE algorithms [21]. The flow-property values at volume faces contained in the convective fluxes which arise from the finite-volume integration process are approximated by the quadratic upstream-weighted interpolation scheme QUICK [22].

Though the present case is a steady state solution, it was found that using a time marching process, with the CFL number being 1, will enhance stability. The solution process consists of a sequential algorithm in which each of the seven sets of equations, in linearised form, is solved separately by application of an alternate-direction tri-diagonal line-implicit solver. The number of ADI sweep adopted in each equation is 5, except in the pressure correction equation, in which the number of sweep employed is 10.

It was found that the employment of the third order approximation of the surface derivatives arising from the viscous and pressure diffusion processes is essential in reproducing the correct flow near-wall asymptotic behavior, by ensuring that the derivative is evaluated right at the surface. Convergence was judged by monitoring the magnitude of the absolute residual sources of mass, momentum and temperature, normalised by the respective inlet fluxes. The solution was taken as having converged when all above residuals fell below 0.01%.

5. Results and discussions

5.1. Fully developed channel flows

5.1.1. Dynamic field

Before proceeding to the discussion of the performance of the proposed k_θ–$\tilde{\epsilon}_\theta$ model, it is beneficial to examine first the accomplishment of the dynamic k–$\tilde{\epsilon}$ model. The focus here is concentrated on the performance of the model in a simple geometry, i.e. fully developed channel flow at $Re_\tau\,(=U_\tau\delta/\nu)=150$, based on the wall friction velocity U_τ, the channel half width δ and the kinematic viscosity ν. The predicted results are contrasted with the DNS data [7]. Computations with grid densities of sizes 60, 100 and 160, which is non-uniform in the direction normal to the wall, were used to check the grid independence. Preliminary results indicated that the three meshes produced nearly identical results, therefore, the 60 grid was used for all subsequent calculations. To ensure the resolution of the viscous sub-layer, more grid points were clustered in the near wall region, and the first grid node near the wall was generally placed at $y^+ \approx 0.1$. However, it was found that, if the correct asymptotic behavior is to be achieved, the first grid node should be at least located at $y+ \approx 0.01$.

The predicted mean velocity profiles are shown in Fig. 1. For comparison purposes, the predicted results by the commonly adopted low Reynolds number models of Launder and Sharma [referred as LS [23], and of Chien [referred as CH] [24] are also included. By observing Fig. 1, it can be seen that predicted velocity by the present model achieves reasonable agreement with the DNS data, though there is a slight underprediction of the U^+ at about $y^+ = 100$. The predicted turbulence kinetic energy and its dissipation rate are shown in Figs. 2 and 3. The superior performance of the proposed dynamic model can be clearly seen from the predicted level of turbulence dissipation rate with the correct maximum level of the property locating at the wall. The correct level of k and ϵ predicted by the proposed dynamic model, ensures the correct dynamic time scale, k/ϵ returned by the model.

The performance of the dynamic model to the elevated Reynolds numbers are further examined. Fig. 4 shows the variation of the predicted skin-friction coefficient C_f with the Reynolds number Re_m, which is

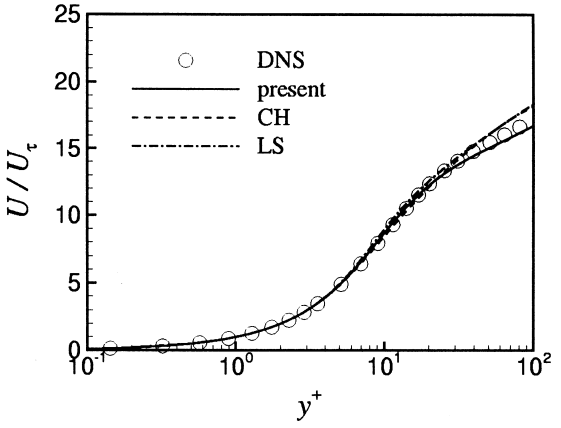

Fig. 1. Mean velocity distribution $Re_\tau = 150$.

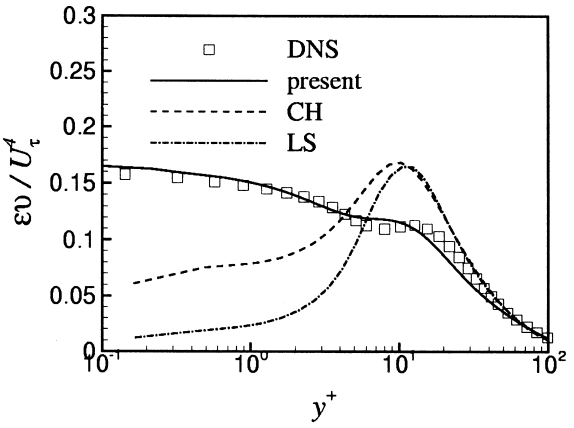

Fig. 3. Turbulent dissipation rate distribution $Re_\tau = 150$.

based on the bulk velocity and channel height. The predicted skin-friction coefficients are scrutinised by comparing the predicted results with two empirical formulae [26,27]. It can clearly be seen that the predicted results agree well with the Dean's formula at $Re_m < 10^5$ and Zarbi's results at $Re_m > 10^5$. The validity of the proposed dynamic model to elevated Reynolds number is further ascertained.

5.1.2. Thermal field with internal heat source

The performance of the proposed k_θ–$\tilde{\epsilon}_\theta$ model is then contrasted with the DNS data [1] of the fully developed channel flow with constant wall temperature and internal heat source at $Re_\tau = 180$, based on the wall friction velocity U_τ, the channel half width δ and the kinematic viscosity ν. DNS results with three different Prandtl numbers, $Pr = 0.1$, 0.71 and 2.0, were reported [1].

Predicted temperature profiles with various Prandtl number fluids are presented in Fig. 5. With decreasing Prandtl numbers, one can see an expansion of the region where $\Theta^+ = Pr\ y^+$ holds, which indicates the thickening of the conductive sublayer. Ultimately, at very low Prandtl numbers, the logarithmic region disappears. But when Pr is near unity, the logarithmic region prevails. The proposed model delivers reasonable predictions of the variations of the temperature profiles by changing the Prandtl number.

By reference to Fig. 6, which shows the predicted turbulent heat flux, it can be observed that the location of the peak value moves further away from the wall, when the Prandtl number decreases. Similar trends can also be seen in the temperature variance results, shown in Fig. 6, in which the thickening of the thermal sublayer is apparent in the low Prandtl number fluid. These trends are well captured by the proposed model. The predicted temperature variance is also compared

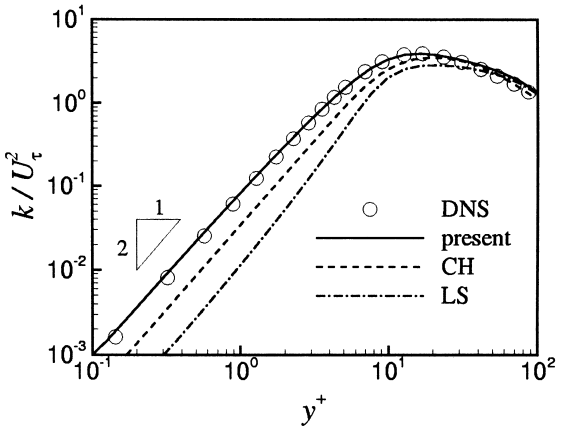

Fig. 2. Turbulent kinetic energy distribution $Re_\tau = 150$.

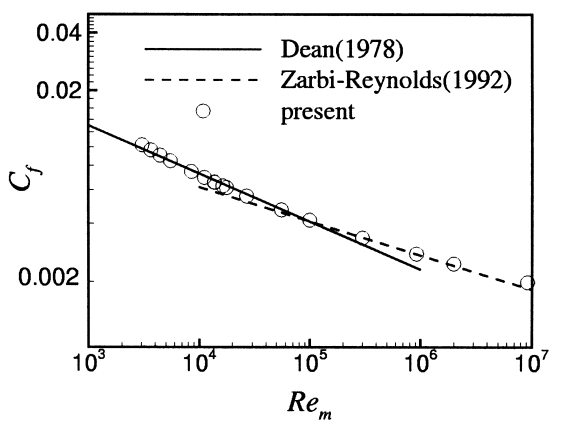

Fig. 4. Friction coefficient of channel flows.

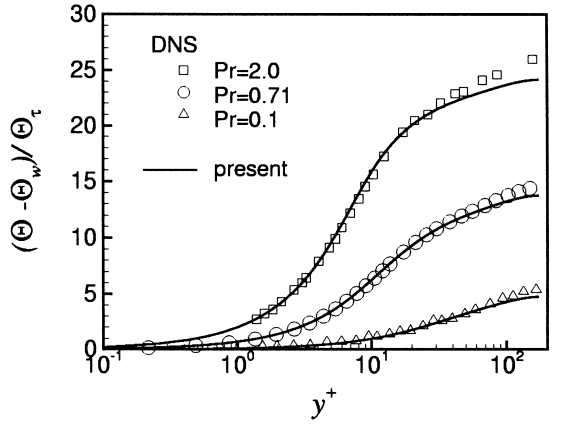

Fig. 5. Mean temperature distributions with different Prandtl number.

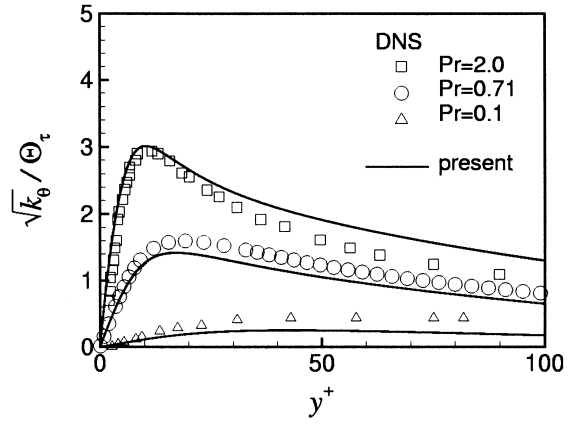

Fig. 7. Temperature variance distributions with different Prandtl number.

favorably with the DNS data, shown in Fig. 7. Fig. 8 shows the predicted turbulent Prandtl numbers' distributions. It can be clearly seen that the Prandtl number is not constant, and the prediction is in reasonable agreement with the DNS data in the near wall region.

The overall performance of the model can be evaluated by examining the predicted budget of temperature variance of $Pr = 0.71$, shown in Fig. 9. It should be pointed out that DNS data at $Re_\tau = 180$ [6] lack detailed k_θ budget, therefore the predicted results are compared with the DNS results [7] at $Re_\tau = 150$. The predicted results show good agreement with DNS data. Both predictions and DNS indicate that the k_θ budget is in general dominated by the production and dissipation away from the wall. In the vicinity of the wall, the dissipation rate balances the viscous diffusion process. It should be pointed out, while most models predicted a misplaced maxima of the dissipation rate ϵ_θ, the proposed model predictions indicate that ϵ_θ is maximum at the wall and this agrees what the DNS data show. This success is partly attributed to the satisfaction of the asymptotic limits in the vicinity of the wall.

5.1.3. Prandtl and Reynolds number effects on Nusselt number

This section addresses the capability of the proposed model to mimic the responses of the Nusselt number to the variation of the Prandtl number and Reynolds number in the fully developed channel flows. Fig. 10 shows the changes of the Nusselt number to the variation of the Prandtl number at $Re_\tau = 150$. The empirical function for pipe flows [28] is also included for comparison. The Prandtl number dependence is well captured by the present model, and the constant turbulent Prandtl number approach fails at low Prandtl number. The capability of the model to predict the

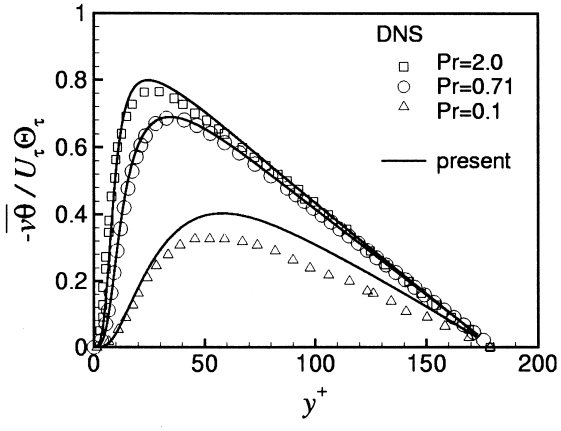

Fig. 6. Turbulent heat flux distributions with different Prandtl number.

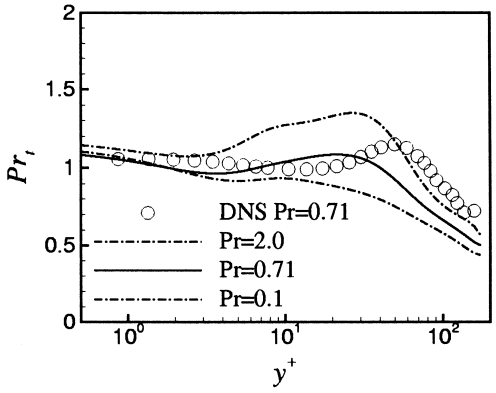

Fig. 8. Turbulent Prandtl number distributions with different Prandtl number fluids.

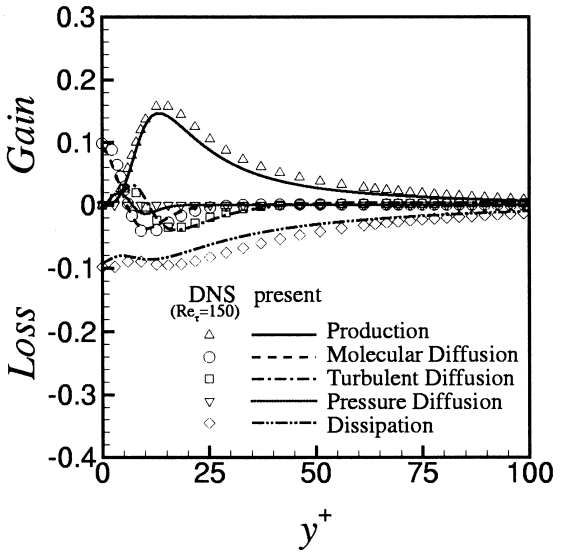

Fig. 9. Budget of temperature variance at $Pr = 0.71$.

Reynolds number dependence on the Nusselt number in the fully developed channel flow is further examined and the cases considered are with Prandtl number at $Pr = 0.022$. Fig. 11 shows a comparison between predicted Nusselt numbers and experimental data [29,30]. Again, the Reynolds number dependence of the Nusselt number is also well predicted by the proposed model.

5.2. Flow with wall transpiration

The adoption of wall transpiration as a flow control technique is frequently encountered in a variety of engineering applications. As a result of fluid injection into the mainstream, a thicker boundary layer is created and consequently the surface skin friction, and hence, drag decreases. Suction, on the other hand, is frequently used to delay the boundary-layer separation and to inhibit the transition to turbulence. Even though the magnitude of the transpiration rate is often low compared to the mainstream, it does significantly change the surface skin friction as well as turbulence quantities near the wall.

Therefore, the performance of the proposed k_θ–$\tilde{\epsilon}_\theta$ model is further contrasted with the DNS data of channel flows with wall transpiration [8] The schematic picture of the flow is shown in Fig. 12. The Reynolds number Re_τ, based on the wall friction velocity U_τ and the channel half-width δ, was set to be 150, where U_τ is the averaged wall shear stress on the two walls. The mass flux ratios on both walls were $F = v_0/U_m = 0.00344$, in which v_0 is the wall-normal velocity and U_m is the axial bulk mean velocity.

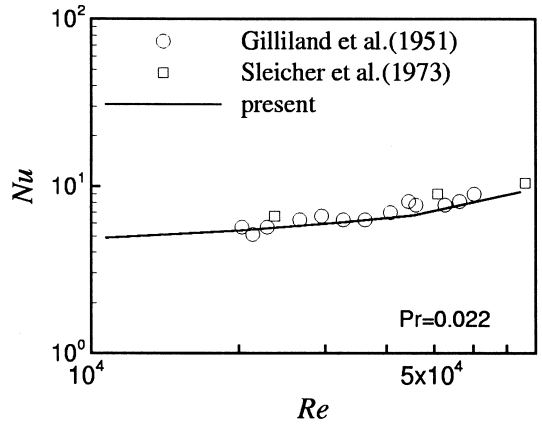

Fig. 11. Nusselt number distributions at different Reynolds number.

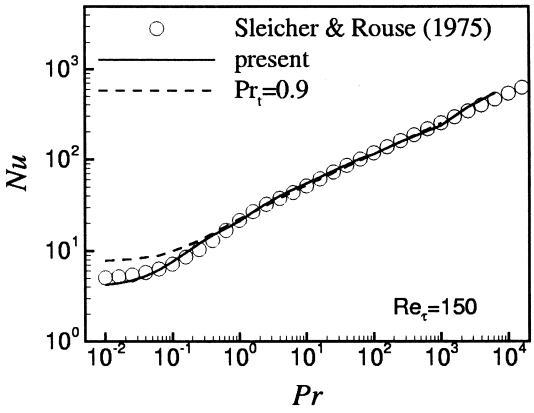

Fig. 10. Nusselt number distributions at different Prandtl number.

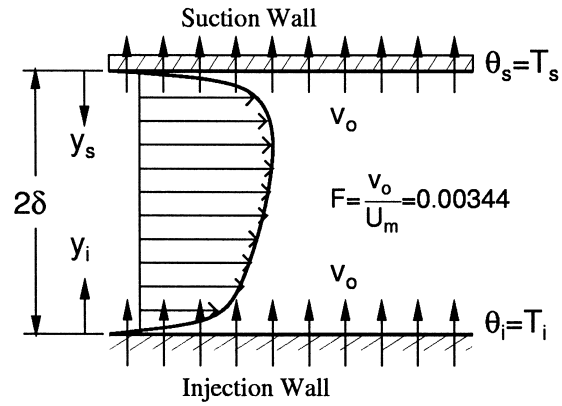

Fig. 12. Geometry of channel flow with wall transpiration.

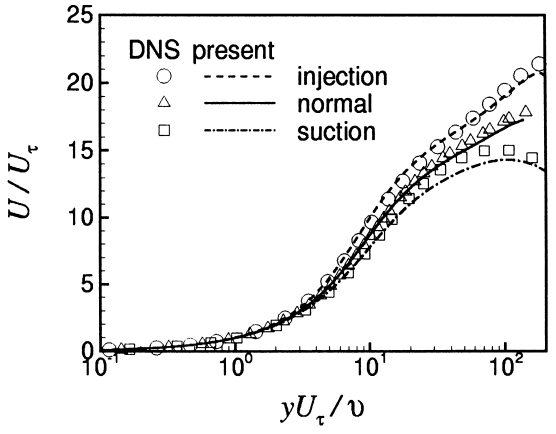

Fig. 13. Mean velocity distribution.

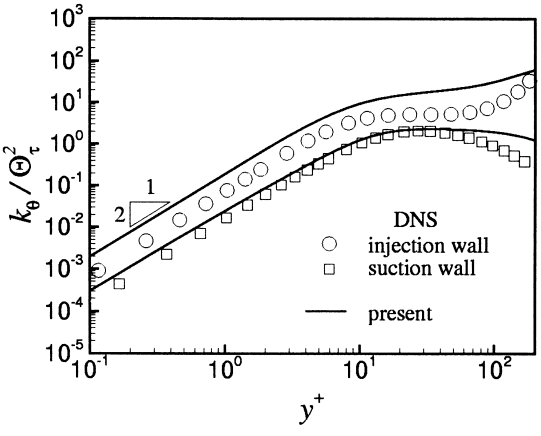

Fig. 15. Temperature variance distribution.

The influence of the wall transpiration on the flow can be seen from the velocity distribution, shown in Fig. 13. For comparison, the $Re_\tau = 150$ DNS data [25] in a fully developed channel flow without wall transpiration are also shown in the figure. A marked different distribution to that without wall transpiration is observed, and the predicted profile agrees well with the DNS distribution. The effect of wall transpiration on the thermal field can be perceived by examining the temperature distributions, as shown in Fig. 14. The near wall variations of the temperature profile are in reasonable agreement with the DNS data.

The asymptotic behaviors of k_θ and $\overline{v\theta}$ in the near-wall region of the injection and suction wall, are shown in Figs. 15 and 16. The results indicate that the present model predicts the correct limiting behaviors, satisfying the quadratic or cubic variation of the turbulent quantities, i.e. $k_\theta \sim y^2$, and $-\overline{v\theta} \sim y^3$. As shown in Figs. 15 and 16, the present model reproduces these relations accurately and gives good agreement with the DNS data. Notably the proposed model is with an unsophisticated form and the success is partly attributed to the satisfaction of the correct near wall asymptotic behaviors.

It is always beneficial to look into the budget of temperature variance at both of the walls to gain further insight of the model performance. Figs. 17 and 18 show the k_θ budget at the injection and suction sides, respectively. Again, both predictions and DNS indicate the k_θ budget is in general dominated by the production and dissipation away from the wall. In the vicinity of the wall, the dissipation rate balances the viscous diffusion process. However, the distributions of the near wall dissipation rate ϵ_θ on the injection and suction wall are somewhat different, as indicated by the DNS data. The energy budget at the suction side is similar to that of the previously examined fully developed flow with internal heat source, shown in Fig. 9.

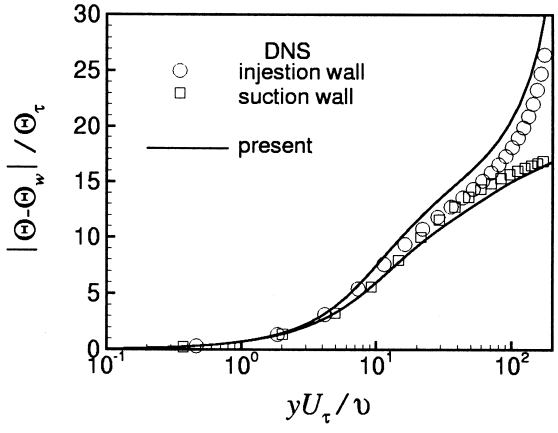

Fig. 14. Mean temperature distribution.

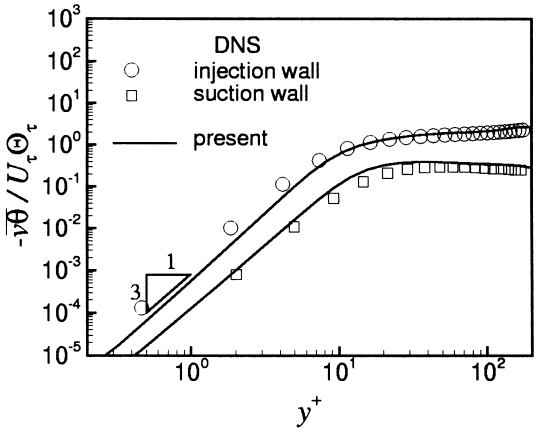

Fig. 16. Turbulent heat flux distribution.

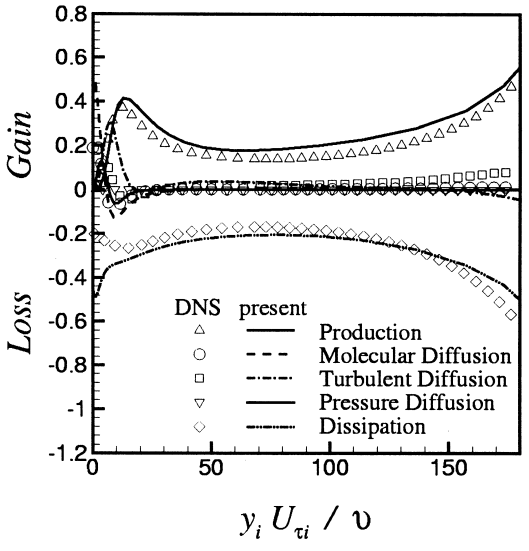

Fig. 17. Budget of temperature variance at injection side.

The local maximum of ϵ_θ is located at the wall itself. At the injection wall, fair agreement with the DNS data is achieved. However, the predicted value of the dissipation rate of temperature variance does not reproduce the decrease of the ϵ_θ when the wall is approached, as indicated by the DNS data. Instead, the predicted result still produces a local maximum at the wall. The prediction seems to generate a too high level of turbulent diffusion towards the wall. It should be pointed out that the ratio of near wall dissipation rate $\epsilon_{\theta_{\text{suction}}}/\epsilon_{\theta_{\text{injection}}}$ is about 25. This can not be observed explicitly from Figs. 17 and 18, because the energy budgets are normalised using the local friction velocity (U_τ) and friction temperature (Θ_τ), which are different at the suction and injection walls. Therefore, the absolute values of terms in Fig. 17 are much smaller than those in Fig. 18.

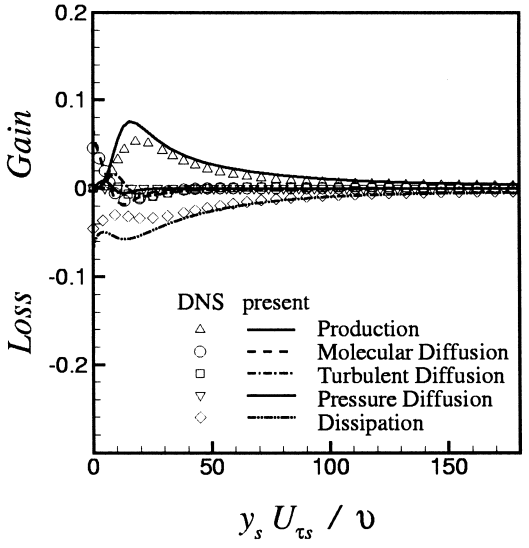

Fig. 18. Budget of temperature variance at suction side.

5.3. Thermal entrance region of a duct

To further explore the model's performance in complex environments, the model is applied to simulate flow in a two-dimensional duct flow, heated with constant wall temperature. Measurements [31] of the wall heat transfer coefficient are available to evaluate the model's performance. The geometry of the duct is shown in Fig. 19. Flows with Reynolds number, $Re_m = 2hU_{m0}/\nu = 6000$, were investigated, where h is the channel height, U_{m0} is the average inlet streamwise velocity and ν is the kinematic viscosity.

A fully developed flow enters from the left hand side of the channel. At $x < 0$, both the top and bottom walls are heated with the same temperature T_0, but at $x > 0$ the bottom wall temperature experiences a sudden change, as indicated in Fig. 19. Therefore, a thermal entrance region exists. This case provides a critical evaluation of the model performance, because the dynamic and thermal fields are not similar, and hence the Reynolds analogy is strictly not applicable. Therefore, it can be expected that the constant turbulent Prandtl approach should fail. By reference to Fig. 20, which shows the Nusselt number distributions at the bottom wall, it can be seen that the present model reproduces the correct Nusselt number distribution, and in contrast a lower level of Nu is predicted by the constant turbulent Prandtl number approach.

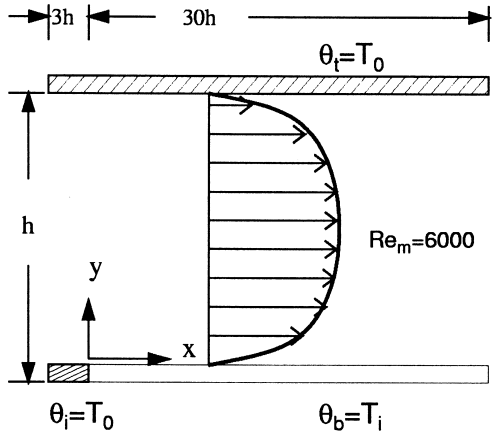

Fig. 19. Geometry of channel flow with thermal entrance region.

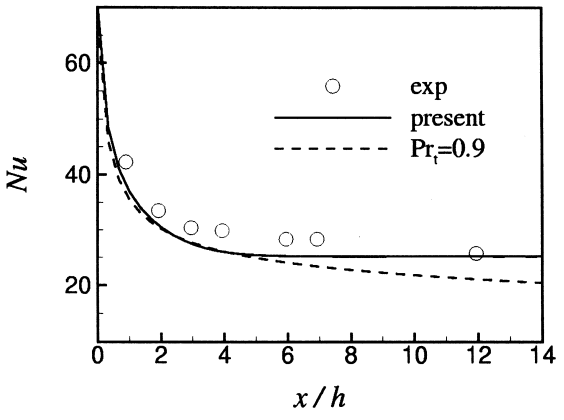

Fig. 20. Nusselt number distribution.

6. Conclusion

A low Reynolds number two-equation k_θ–$\tilde{\epsilon}_\theta$ turbulence model is proposed to predict thermal field without the explicit prescription of the turbulent Prandtl number. The design of the model is to possess correct asymptotic behavior in the vicinity of the wall, and the asymptotic limits of the k_θ and $\tilde{\epsilon}_\theta$ equations are satisfied by the incorporation of the viscous dissipation related terms. Cases considered are fully developed channel flows, with and without wall transpiration, and the thermal entrance region of a duct. The performance of the proposed model is contrasted with the DNS data of the fully developed channel flow with and without wall transpiration. For the nonpermeable wall, but with internal heat source case, the proposed model delivers reasonable predictions of the variations of the temperature profiles to the changes of the Prandtl number. The effect of the presence of wall transpiration on the thermal field is also correctly reproduced by the prediction and is in good agreement with the DNS data. Finally, the predicted Nusselt number distribution of a developing thermal field is compared favorably with measurements.

Acknowledgements

This research work was supported by the National Science Council of Taiwan under grant NSC-85-2212-E-007-057 and the computational facilities were provided by the National Centre for High-Performance Computing of Taiwan which the authors gratefully acknowledge.

References

[1] J. Kim, P. Moin, Transport of passive scalars in a turbulent channel flow, Turbulent Shear Flows 6 (1989) 85–96.

[2] R.A. Antonia, J. Kim, Turbulent Prandtl number in the near-wall region of a turbulent channel flow, International Journal of Heat and Mass Transfer 34 (1991) 1905–1908.

[3] T.P. Sommer, R.M.C. So, Y.G. Lai, A near-wall two-equation model for turbulent heat fluxes, International Journal of Heat and Mass Transfer 35 (1992) 3375–3387.

[4] B.E. Launder, Numerical computation of convective heat transfer in complex turbulent flows: time to abandon wall functions?, International Journal of Heat and Mass Transfer 27 (1984) 1485–1491.

[5] T. Nagano, C. Kim, A two-equation model for heat transport in wall turbulent shear flows, Journal of Heat Transfer 110 (1988) 583–589.

[6] N.N. Mansour, J. Kim, P. Moin, Reynolds-stress and dissipation rate budget in a turbulent channel flow, Journal of Fluid Mechanics 194 (1988) 15–44.

[7] N. Kasagi, Y. Tomita, A. Kuroda, Direct numerical simulation of passive scalar field in a turbulent channel flow, ASME Journal of Heat Transfer 114 (1992) 598–606.

[8] Y. Sumitani, N. Kasagi, Direct numerical simulation of turbulent transport with uniform wall injection and suction, AIAA Journal 33 (1995) 1220–1228.

[9] C.B. Hwang, C.A. Lin, Improved low Reynolds number $k--\epsilon$ model based on direct numerical simulation data, AIAA Journal 36 (1998) 38–43.

[10] H. Kawamura, A $k--\epsilon--$v2 model with special relevance to the near wall turbulence, in: Proceeding of the 8th Symposium on Turbulent Shear Flow, 1991, pp. 26.4.1–26.4.6.

[11] B.E. Launder, Heat and mass transport, Topics in Applied Physics 12 (1976) 231–287.

[12] W.P. Jones, B.E. Launder, The calculation of low Reynolds number phenomena with a two-equation model of turbulence, International Journal of Heat and Mass Transfer 16 (1973) 1119–1130.

[13] Y. Nagano, M. Simada, Modeling the dissipation-rate equation for two-equation turbulence model, in: Proceeding of the 9th Symposium on Turbulent Shear Flow, 1993, pp. 32.2.1–32.2.6.

[14] Y. Nagano, M. Tagawa, An improved k–ϵ model for boundary layer flows, Journal of Fluids Engng 112 (1990) 33–39.

[15] M.S. Youssef, Y. Nagano, M. Tagawa, A two-equation heat transfer model for predicting turbulent thermal fields under arbitrary wall thermal conditions, International Journal of Heat and Mass Transfer 35 (1992) 3095–3104.

[16] K. Horiuti, Assessment of two-equation models of turbulent passive-scalar diffusion in channel flow, Journal of Fluid Mechanics 238 (1992) 405–433.

[17] S.E. Elghobashi, B.E. Launder, Turbulent time scale and the dissipation rate of temperature variance in the thermal mixing layer, Physics of Fluids 26 (1983) 2415–2419.

[18] H. Kawamura, H. Ihira, DNS and modeling of scalar transport in homogeneous turbulence, in: W. Rodi, G. Bergeles (Eds.), Engineering Turbulence Modelling and Experiments 3, 1996, pp. 239–248.

[19] H. Kawamura, Y. Wakao, Modelling of scalar transport in a turbulent channel flow consistent with the linearity principle, in: 10th Symposium on Turbulent Shear Flows, 1995.
[20] C.A. Lin, M.A. Leschziner, Three-dimensional computation of transient interaction between radially injected jet and swirling cross-flow using second-moment closure, Computational Fluid Dynamics Journal 1 (1993) 423–432.
[21] S.V. Patankar, Numerical Heat Transfer and Fluid Flow, Chapters 6 & 7, Hemisphere Publishing Corporation, 1980.
[22] B.P. Leonard, Stable and accurate convective modelling procedure based on quadratic upstream interpolation, Computer Methods in Applied Mechanics and Engineering 19 (1979) 59–98.
[23] B.E. Launder, B.I. Sharma, Application of the energy dissipation model of turbulence to the calculation of flow near a spinning disc, Letters in Heat and Mass Transfer 1 (1974) 131–138.
[24] K.Y. Chien, Predictions of channel and boundary layer flows with a low Reynolds number turbulence model, AIAA Journal 20 (1982) 33–38.
[25] A. Kuroda, N. Kasagi, M. Hirata, Direct numerical simulation of turbulent plane Couette-Poiseuille flows: effect of mean shear on the near wall turbulence structure, in: Proceeding of the 9th Symposium on Turbulent Shear Flow, 1993, pp. 8.4.1–8.4.6.
[26] R.B. Dean, Reynolds number dependence of skin friction and other bulk flow variables in two-dimensional rectangular duct flow, Trans. ASME Journal of Fluids Engineering 100 (1978) 215.
[27] G. Zarbi, A.J. Reynolds, Wall stress measurements in two-dimensional turbulent channel and boundary-layer flows, and the wall layer differences, Trans. Japan Society of Mechanical Engineering B58 (1992) 1378.
[28] C.A. Sleicher, M.W. Rouse, A convenient correlation for heat transfer to constant and variable property fluids in turbulent pipe flow, International Journal of Heat and Mass Transfer 18 (1975) 677–683.
[29] C.A. Sleicher, A.S. Awad, R.H. Notter, Temperature and eddy diffusivity profiles in NaK, International Journal of Heat and Mass Transfer 16 (1973) 1565–1575.
[30] E.R. Gilliland, R.J. Musser, W.R. Page Heat Transfer to Mercury, in: General Discussion on Heat Transfer, Institute of Mechanical Engineering and ASME, London, 1951, pp. 402–404.
[31] A.K. Abdel-Rahman, Y. Hagiwara, K. Suzuki, Turbulent flow and heat transport in a duct with fluid injection from wall, in: Proceeding of the 9th Symposium on Turbulent Shear Flow, 1993, pp. 18.4.1–18.4.6.